

Magnetic order, metamagnetic transitions, and low-temperature spin freezing in $\text{Ca}_3\text{Co}_2\text{O}_6$: an NMR study.

G. Allodi,^{1,*} R. De Renzi,¹ S. Agrestini,^{2,3} C. Mazzoli,^{4,5} and M. R. Lees⁶

¹*Dipartimento di Fisica e Unità CNISM, Università degli Studi di Parma, Viale G. Usberti 7A, I-43100 Parma, Italy*

²*Laboratoire CRISMAT, UMR 6508, Boulevard du Maréchal Juin, 14050 Caen Cedex, France*

³*Max Planck Institute for Chemical Physics of Solids, Nöthnitzerstr. 40, 01187 Dresden, Germany*

⁴*European Synchrotron Radiation Facility, BP 220, 38043 Grenoble Cedex 9, France*

⁵*Dipartimento di Fisica, Politecnico di Milano, Piazza Leonardo da Vinci 32, I-20133 Milano, Italy*

⁶*Department of Physics, University of Warwick, Coventry, CV4 7AL, United Kingdom*

(Dated: October 21, 2019)

We report on a ^{59}Co NMR investigation of the trigonal cobaltate $\text{Ca}_3\text{Co}_2\text{O}_6$ carried out on a single crystal, providing precise determinations of the electric field gradient and chemical shift tensors, and of the internal magnetic fields at the non-magnetic CoI sites, unavailable from former studies on powders. The magnetic field-induced ferri- and ferromagnetic phases at intermediate temperature (e.g. 10 K) are identified by distinct internal fields, well accounted for by purely dipolar interactions. The vanishing transferred hyperfine field at the CoI site indicates that the Co^{3+} (I) orbitals do not participate in the intra-chain superexchange, in disagreement with a previous theoretical model.

The strong Ising character of the system is confirmed experimentally by the field dependence of the resonance lines, indicating that local moments are saturated even at the phase boundaries. In the vicinity of the critical fields, nuclear spin-spin relaxations detect the spin reversal dynamics of large magnetic assemblies, either Ising chain fragments or finite size domains, which drive the metamagnetic transitions. Such collective excitations exhibit a glassy behavior, slowing down to subacoustic frequencies and freezing at low temperature. The relevance of such slow fluctuation modes for the low-temperature multi-step behavior reported in the magnetization is discussed.

PACS numbers: 75.30.Kz, 75.30.Et, 75.60.Jk, 76.60.-k.

I. INTRODUCTION

The nature of magnetic order in the geometrically frustrated trigonal cobaltate $\text{Ca}_3\text{Co}_2\text{O}_6$, an Ising-type magnet exhibiting low-dimensional behavior, has been a puzzle for over a decade. The crystal structure of $\text{Ca}_3\text{Co}_2\text{O}_6$ (Fig. 1) may be viewed as the result of the alternate stacking along the c axis of face-sharing CoO_6 octahedra (CoI) and CoO_6 trigonal prisms (CoII) with a rather short CoI - CoII distance $c/4 = 2.59 \text{ \AA}$, building up *chains* arranged over the ab plane in a triangular lattice, with a much larger spacing (inter-chain distance $a/\sqrt{3} = 5.24 \text{ \AA}$).^{1,2} The Co^{3+} oxidation state at both sites is now established,^{3,4} contrary to earlier predictions for a Co^{2+} - Co^{4+} charge disproportionation.⁵

Magnetism resides on the CoII site, where a trigonal crystal field yields a high-spin ground state with a large unquenched orbital component ($\langle L_z \rangle \approx 1.7$, $\langle 2S_z + L_z \rangle = 5.3$), while CoI is in a low-spin state (i.e. non-magnetic).³ Spin-orbit coupling gives rise to a single-ion anisotropy term $-DS_z^2$ of order 70 meV (corresponding to an anisotropy field $B_{anis} \approx 200 \text{ T}$ along c), whence the strong Ising-type character of magnetism in this system.^{2,6} Exchange coupling between the Co^{3+} II ions is ferromagnetic (FM) and relatively strong along the chains, whereas it is antiferromagnetic (AF) and much weaker between chains. While the dominant intra-chain exchange interaction promotes quasi one-dimensional Ising-type ferromagnetism, the actual magnetic structure is the result of the competing residual

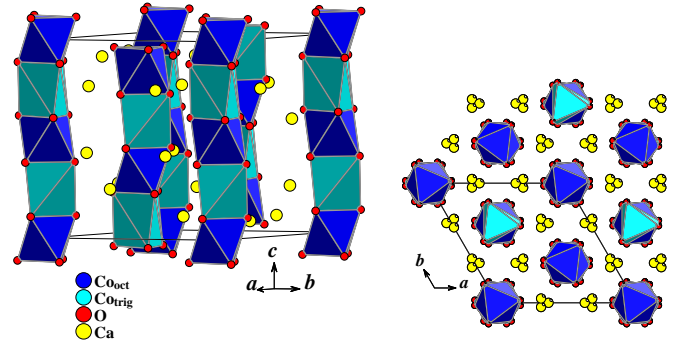


FIG. 1: (Color online) Lattice structure of $\text{Ca}_3\text{Co}_2\text{O}_6$ in the hexagonal setting. Left: perspective view of the spin chains formed by the CoO_6 polyhedra along the c -axis; right: cross-section in the ab plane, evidencing the arrangement of chains in the triangular lattice. The dark and light polyhedra represent the CoO_6 octahedra and CoO_6 trigonal prisms, respectively.

inter-chain AF coupling, giving rise to a complex magnetic phenomenology as a function of temperature and magnetic field.

Susceptibility measurements actually demonstrate the onset of magnetic order at $T < T_c \approx 25 \text{ K}$.^{2,7} The nature of magnetic ordering however, has been the subject of a long-lasting controversy. Denoting spin-up, spin-down, or magnetically disordered Ising chains as $\uparrow, \downarrow, 0$, respectively, theoretical models indicated either a ferrimagnetic (FI) $[\uparrow\uparrow\downarrow]$ or a partially disordered antiferromagnetic

(PDA) structure $[\uparrow\downarrow 0]$ as the stable zero-field arrangements of the three inequivalent chains on the triangular lattice in the presence of geometrically frustrated AF inter-chain coupling.^{8,9} Early neutron diffraction experiments seemingly supported either a PDA¹⁰ or a FI⁷ order, although poor quantitative agreement of both structures with magnetic peak intensities was later pointed out.¹¹ Recent x-ray¹² and neutron scattering¹³ data on single crystals have revealed the incommensurate character of the magnetic order in this compound. They show that the actual structure, referred to as *modulated PDA* (MPDA), rather consists of long-wavelength longitudinal spin-density modulations along each chain, phase-shifted by $\pm 2\pi/3$ with respect to the neighboring chains.¹³ Nevertheless, the MPDA phase is apparently metastable below 14 K, as indicated by the decrease in the intensity of the MPDA magnetic peaks.^{11–13}

The nature of the magnetic order in an externally applied magnetic field is also far from clear. Increasing magnetic fields applied along c tend to stabilize the FI phase and eventually FM inter-chain order. At $5\text{ K} < T < T_c$, the initial saturation of the magnetization to a magnetic moment $M_{FI} \approx 1.7\mu_B$ per formula unit at $\mu_0 H > B_{c1} \approx 0.1\text{ T}$, followed by a step to $M_{FM} \approx 3M_{FI}$ at $\mu_0 H > B_{c2} \approx 3.5\text{ T}$, actually points to perfect FI and FM phases below and above H_{c2} , respectively. However, the $M(H)$ curves at lower temperatures display a puzzling multi-step behavior reminiscent of the quantum tunneling of magnetization detected in molecular magnets.^{14,15} A number of complex magnetic superstructures, distinct from both the FI and FM spin-chain arrangements, have been proposed in order to explain the fractional magnetization values. However, such superstructures cannot account for all the plateaus observed in $M(H)$.¹⁶

In this paper, we address the issue of the field-dependent magnetic order of $\text{Ca}_3\text{Co}_2\text{O}_6$ by means of ^{59}Co nuclear magnetic resonance (NMR). Previous ^{59}Co NMR research on $\text{Ca}_3\text{Co}_2\text{O}_6$ polycrystalline samples, though successful in demonstrating the presence of non-magnetic Co^{3+} , could only provide very limited information on the magnetic structure, due to the angular averaging of the complex multi-line quadrupolar spectra into broad powder patterns.⁴ The FM and FI surroundings, on the contrary, can be clearly resolved in our NMR investigation of a high-quality single crystal, while the two field-induced transitions, namely MPDA-FI and FI-FM, were precisely identified at 10 K through step-like jumps in the internal field and peculiar features of the spin-spin relaxations, indicative of glassy spin dynamics. Our study also yields a detailed characterization of the chemical shift and the electric field gradient (EFG) tensors at the non-magnetic CoI site.

The paper is organized as follows. Sample preparation and the experimental methods are briefly described in section II. NMR spectra, providing information on the magnetic structures, and nuclear relaxation data, probing the dynamical excitations of the spin system, are pre-

sented in sections III A, and III B, respectively. The calculated dipolar fields at the CoI sites in the FI and FM phases are compared with experimental values in section IV. The results are discussed in section V. Two appendices review in some detail the complex dependence of the ^{59}Co resonances on magnetic and quadrupolar interactions, and the longitudinal relaxation function of a $7/2$ nuclear spin.

II. EXPERIMENT

The investigated sample was a single crystal of size $1.2 \times 1.2 \times 5.8\text{ mm}^3$ (the long side parallel to the c axis) taken from a batch of several needle-shaped crystals obtained by the flux method. The crystals were grown using the following procedure: a mixture of $\text{Ca}_3\text{Co}_2\text{O}_6$ powder and KCO_3 (the flux), in a weight ratio 1/7, was heated up to 990°C in an alumina crucible for one hour and then slowly cooled down to room temperature. A sample of the same batch was employed for the resonant x-ray scattering study of Ref. 12. The high quality of the crystals was confirmed by preliminary x-ray diffraction, energy dispersive x-ray, magnetization, and specific heat measurements.

Magnetization measurements were performed after zero field cooling, by using a vibrating sample magnetometer (Oxford Instruments) equipped with a 12 T magnet, with a field sweep rate of 1 T/min in order to minimize any relaxation effect. Susceptibility measurements were carried out by means of a superconducting quantum interference device magnetometer (SQUID) with magnetic fields up to 5 T and temperatures down to 1.8 K (Quantum Design MPMS). The magnetic measurements were carried out for the two geometries corresponding to the magnetic field applied parallel or perpendicular to the c axis, i.e. parallel or perpendicular the direction of the chains and the spins. In the case of parallel geometry the crystals were aligned using the magnetic field itself at 5 T as explained in Ref. 17. The alignment of the crystals in the perpendicular geometry can be easily obtained thanks to their rod-like shape.

The NMR experiments were performed by means of a home-built phase-coherent pulsed spectrometer¹⁸ and a fast-sweeping cold-bore cryomagnet (Oxford Instruments EXA) equipped with a variable temperature insert as a sample environment. The crystal was mounted on a sample rotator, providing an angular span of $\pm 120^\circ$ with respect to the applied field. Misalignment of the rotation axis (nominally perpendicular to the field) was estimated not to exceed 5 degrees. In the case of the c axis parallel to the field, however, a precise alignment of the sample was achieved, thanks to its large magnetic anisotropy, by loosely mounting it in the coil.

NMR spectra were detected by exciting spin echoes by means of a standard $P - \tau - P$ sequence, with equal rf pulses P of duration 3–5 μs and intensity suitably regulated for optimum signal, and delays τ kept as short

as possible with respect to the dead time of the resonant probehead ($\approx 10\text{-}25\mu\text{s}$ depending on the working frequency). Recording was carried out either by tuning the probehead at discrete frequencies in a constant field (frequency sweep mode), or by varying the applied field and exciting the resonance at a constant frequency (field sweep mode). Although an indirect method, we preferentially employed the latter whenever possible (namely, far from the metamagnetic transitions) as it yields smoother data, independent of the frequency response of the spectrometer, in a fully automated procedure.

Nuclear spin-spin relaxations were determined by the decay of the signal amplitude in the same spin echo sequence $P-\tau-P$, as a function of variable delay τ . Spin-lattice relaxations were measured by the signal recovery following a so-called fast saturation of the observed nuclear transition (see Appendix B), obtained with an aperiodic train of 10-15 pulses.

III. EXPERIMENTAL RESULTS

A. NMR spectra

We report separately the ^{59}Co resonance spectra recorded in the longitudinal geometry (external field $\mathbf{B}_{\text{ext}} \parallel c$ axis), a geometry that allowed us study the field-induced magnetic order in the system, and in transverse applied fields. Interpretation of the spectra is relatively simple and model-independent in the longitudinal case, due to the collinearity of all the fields (internal and external magnetic fields, and the EFG). In the general case, the dependence of the ^{59}Co resonances on magnetic and quadrupolar interactions is rather complex, as recalled in some detail in Appendix A.

1. Longitudinal applied fields

A ^{59}Co NMR signal could be detected below 15 K in moderate longitudinal external magnetic fields $B_{\text{ext}} > 0.1$ T. Such field values assign the system to the FI phase. For such field values the FI phase is induced in the system. In contrast, no signal could be detected in the MPDA phase at $B_{\text{ext}} < 0.1$ T.

A typical frequency-sweep spectrum, recorded at 10 K in 0.38 T, is plotted in Fig. 2. The spectrum consists in a septet of quadrupole-split Zeeman transitions ν_n , $n = -3, \dots, n = 3$ (Eqn. A2), with constant frequency spacing $\nu_{n+1} - \nu_n = 2.11(1)$ MHz, in agreement with Ref. 19. In this geometry ($\theta = 0$), and in the presence of a cylindrical EFG ($\eta = 0$), as is actually the case (see Sec. III A 2), such a line spacing coincides with the quadrupolar coupling parameter ν_Q (Eqn. A3). The resonance frequency ν_0 of the central line, which is unaffected by the quadrupole interaction, corresponds to a field $B_{\text{nuc}} = 2\pi\nu_0/^{59}\gamma$ at the nucleus which is larger than B_{ext} by approximately 1.2 T (here, $^{59}\gamma = 2\pi \times 10.10$ MHz/T²⁰ is the gyromagnetic ratio of ^{59}Co). Such a field offset,

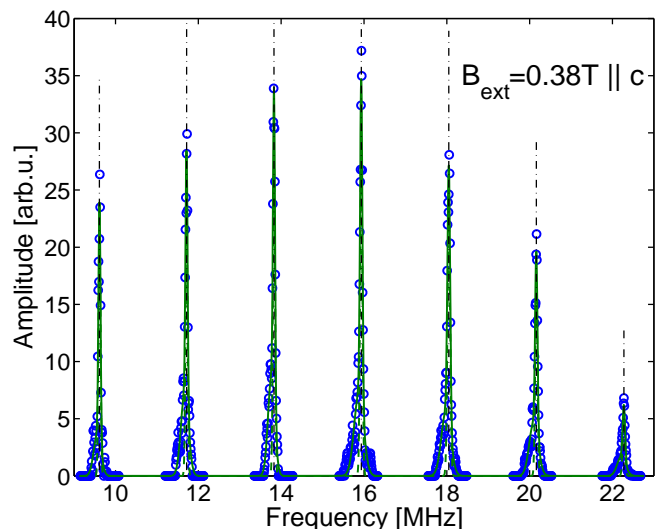


FIG. 2: (Color online) Frequency-swept ^{59}Co spectrum at 10 K from the majority spin-up chains of the FI phase, recorded in a field of 0.38 T applied along the c axis. Solid lines are bimodal fits of the satellite peaks, vertical dash-dotted lines mark their centers of gravity.

though sizable, is nevertheless much smaller than the typical hyperfine fields detected in magnetic Co^{3+} , which are of the order of -10 T/ μ_B and $+60$ T/ μ_B for the spin and orbital hyperfine components, respectively.^{21,22} This confirms that the present ^{59}Co signals are from Co^{3+} ions in a low-spin state, in agreement with previous NMR reports.^{4,19} We note that the dipolar field at site I generated by two nearest-neighbor Co II moments of $5.2 \mu_B$ aligned parallel to \mathbf{B}_{ext} accounts for both the positive sign of the field offset $B_{\text{nuc}} - B_{\text{ext}}$, and its magnitude to within a few percent accuracy. This is the first indication that the internal field $\mathbf{B}_{\text{int}} \approx \mathbf{B}_{\text{nuc}} - \mathbf{B}_{\text{ext}}$ arises from the surrounding magnetic ions essentially through the dipolar coupling, as actually proven in detail by the internal field calculations of Sec. IV. Given its dominant on-chain dipolar origin, the positive sign of B_{int} then indicates that the nearest-neighbor Co^{3+} spins are aligned along the direction of the applied field. The present positive-offset line multiplet therefore originates from nuclei at the Co I sites of spin chains aligned parallel to the external field, namely, the majority chains of the FI structure.

Qualitatively similar positive-offset spectra could be reproduced in increasing external fields parallel to the c axis ($\theta = 0$) at 10 K, up to $B_{\text{ext}} = 3.5$ T. The resonance frequency of the central line follows a linear dependence on B_{ext} (Fig. 3),

$$\nu_0 = aB_{\text{ext}} + b \quad (1)$$

with best-fit parameters $a_{\uparrow} = 10.21(1)$ MHz/T, $b_{\uparrow} = 12.02(2)$ MHz (hereafter, $\uparrow \downarrow$ in the subscripts denote quantities related to spin-up majority and spin-down minority chains of the FI phase, respectively). On the other

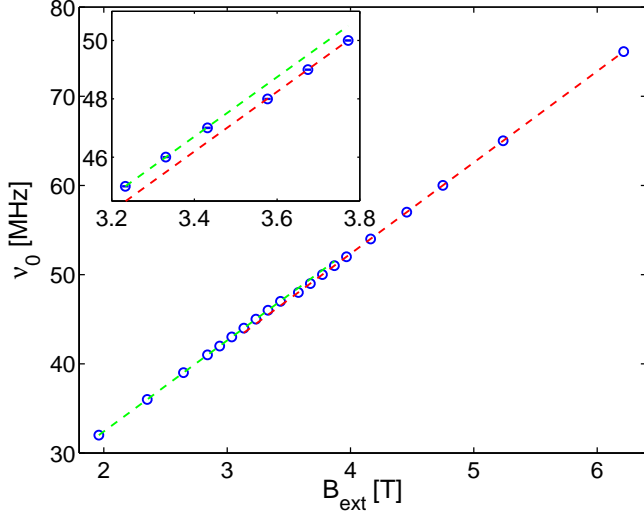


FIG. 3: (Color online) Central resonance frequency ν_0 of the positive-offset spectra from the spin-up chains in either the FI ($B_{ext} < 3.5$ T) or the FM phase ($B_{ext} > 3.5$ T), as a function of $B_{ext} \parallel c$. The dashed lines are fits to straight lines for the two phases. The inset is a blow-up of the transition region.

hand

$$\nu_0 \equiv {}^{59}\gamma B_{nuc} = {}^{59}\gamma(1 + K_c)(B_{ext} + B_{int}) \quad (2)$$

as detailed in Appendix A. If the staggered magnetization is saturated all over the field span, the internal field B_{int} is independent of B_{ext} and, by symmetry, also parallel to c . Working under this hypothesis, whose validity is demonstrated in the discussion, a comparison of Eqs. 1 and 2 simply relates the coefficients a , b to B_{int} and the c axis component of the chemical shift tensor K_c : $a = {}^{59}\gamma(1 + K_c)$, $b = {}^{59}\gamma(1 + K_c)B_{int}$, respectively. Best-fit values for a_{\uparrow} and b_{\uparrow} then yield $B_{int\uparrow} = 1.178(2)$ T, and a sizable $K_c \approx 0.01$.

Resonances from the minority spin-down chains are marked by a negative field offset, comparable in absolute value to the internal field in the majority chains. The signal could only be found in longitudinal fields exceeding 2 T, since for smaller external fields its resonance frequency $\nu_0 \approx {}^{59}\gamma||B_{int}| - |B_{ext}||$ falls below 10 MHz, outside the frequency range of our apparatus. A field sweep spectrum at 10 K, recorded at fixed frequency of 16 MHz, is shown in Fig. 4. It consists of a multiplet of quadrupole-split lines centered at B_n ,²³ similar to those detected for the majority chains, with a central resonance at $B_0 = 2.792$ T. The two satellites at $B_{-2} = 3.172$ T and $B_{-3} \approx 3.36$ T are however reduced in amplitude by approximately 75% and 90% with respect to the symmetric peaks at B_2 , B_3 , respectively. The signal loss at $B_{ext} \geq B_{-2}$ is due to the approach of the FI-FM transition at $B_{c2} \approx 3.5$ T, which is accompanied by a notable relaxation phenomenon that partially wipes out the signal intensity over a wide field interval close to B_{c2} (see below). The rightmost satellite at B_{-3} is

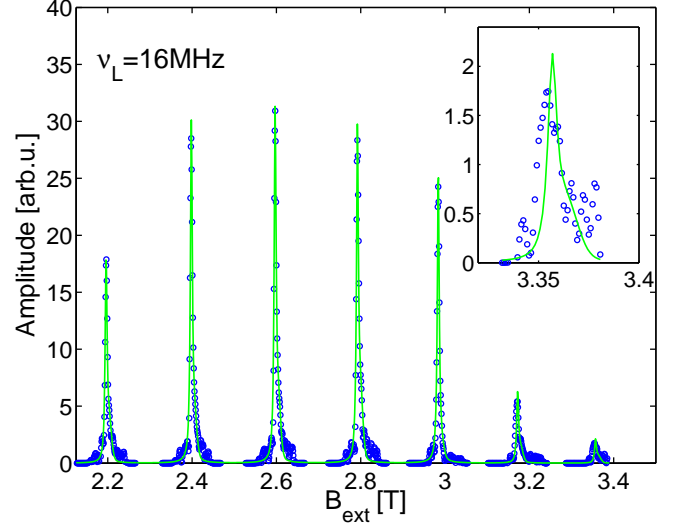


FIG. 4: (Color online) Field-swept spectrum ($B_{ext} \parallel c$) at 10 K from the minority spin-down chains, recorded at a constant frequency $\nu = 16$ MHz. The solid line is a bimodal fit to a septet of quadrupolar satellites, with positions constrained by Eqn. A2. The inset is a blow-up of the rightmost satellite at $B_{-3} \approx 3.36$ T.

furthermore displaced from the expected position by approx. -2 mT (figure inset), a value well accounted for by the demagnetization field, since the macroscopic magnetization significantly deviates from the FI plateau at $H = \mu_0^{-1}B_{-3}$ (Fig. 11). The quadrupole coupling parameter is estimated as $\nu_Q = 1.97(1)$ MHz from the line spacing, $\nu_Q = {}^{59}\gamma(1 + K_c)(B_{n-1} - B_n)$, and is slightly, but significantly smaller than in the spin-up chains.

The resonance frequency of the central line follows a similar linear dependence on B_{ext} (Fig. 5), with slope $a_{\downarrow} = 10.22(1)$ MHz/T, and a negative intercept $b_{\downarrow} = -12.48(3)$ MHz (Eqn. 1). The former coincides within error with a_{\uparrow} , whence the same chemical shift value $K_c \approx 0.01$ is obtained. From b_{\downarrow} , the internal field at CoI in the minority chains is estimated as $B_{int\downarrow} = -1.221(4)$ T.

The negative-offset resonance lines from the minority spin-down chains completely disappear in external fields $B_{ext} > 3.5$ T, while only a positive-offset septet can be detected, that is qualitatively similar to the one from the majority FI chains below 3.5 T and with an identical quadrupole splitting $\nu_Q = 2.11(1)$ MHz (Fig. 6). The integrated amplitudes of the positive-offset spectra above and below 3.5 T, and proportional to the number of ${}^{59}\text{Co}$ nuclei excited in spin-up chains, have a ratio very close to 3:2. These facts indicate that all the spin chains are now aligned parallel to the external field, i.e. the system is in a FM state.

The positive-offset septet from the spin-up chains could be followed at 10 K while increasing B_{ext} in steps of approx. 0.1 T across the field-induced FI-FM transition, without losing the signal. The resonance frequency of the central line is plotted vs. B_{ext} in Fig. 3. Experi-

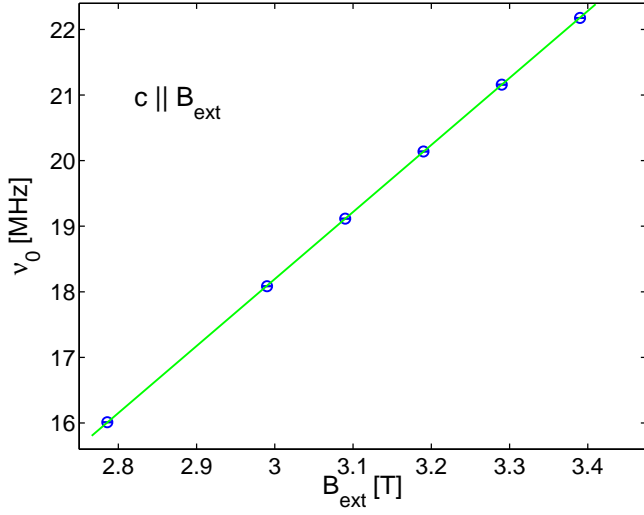


FIG. 5: (Color online) Central resonance frequency ν_0 of the spectra from the minority spin-down FI chains, as a function of $B_{ext} \parallel c$. The solid line is a fit to Eqn. 1.

mental points clearly follow two different straight lines above and below 3.5 T (Eqn. 1), which signals the occurrence of a transition at a critical field $B_{c2} = 3.50(5)$ T. Line parameters on the FM side are fitted as $a^{FM} = 10.23(1)$ MHz/T, in good agreement with the a values in the FI phase, and a reduced $b^{FM} = 11.40(1)$ MHz, corresponding to a step-like decrease of the internal field, $B_{int}^{FM} = 1.115(2)$ T.

The transition is also accompanied by an abrupt broadening by a factor of about 2 of the satellite lines above B_{c2} . A closer inspection of the resonance lines reveals, on both sides of the transition, an asymmetrical bimodal shape with a sharper peak and a broader negatively-shifted shoulder, that is more pronounced in the FM phase. Line shapes and widths, in contrast, are independent of satellite order m . These facts indicate that the observed inhomogeneous broadening is magnetic in origin. The increase in line width $\Delta\nu_L$ above B_{c2} qualitatively agrees with a dominant line broadening from the demagnetization field, which is proportional to its net magnetization, and inhomogeneous throughout the sample due to its non-ellipsoidal shape. The agreement is not quantitative, however, since a step in $\Delta\nu_L$ by a factor of 3 across B_{c2} is expected from the corresponding step in the macroscopic magnetization. Such a discrepancy suggests the presence of an extra broadening mechanism, relatively more important in the FI phase.

2. Transverse applied fields

The crystal was also mounted with its c axis perpendicular to the external field, in order to study the transverse components of the EFG and \hat{K} tensors in an azimuthal scan of B_{ext} in the ab plane. A typical field-sweep spectrum at 10 K, recorded at a fixed frequency $\nu_L = 75.6$ MHz, is shown in Fig. 7. The spectrum con-

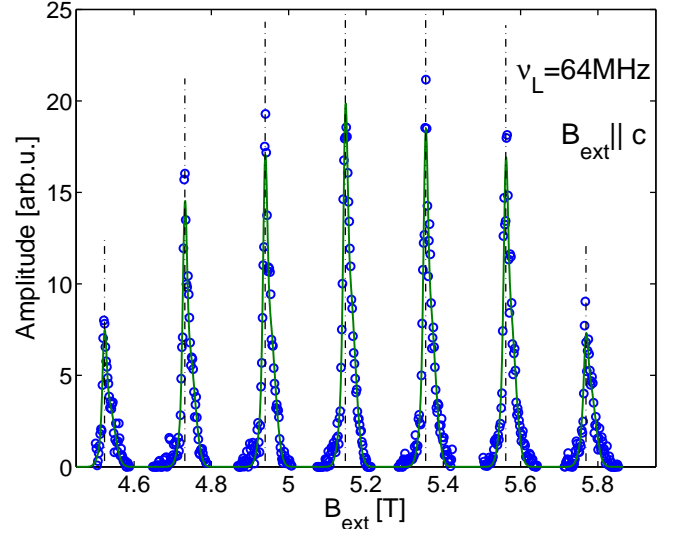


FIG. 6: (Color online) Field-swept ($B_{ext} \parallel c$) ^{59}Co spectrum in the FM phase at 10 K, recorded at a constant frequency $\nu = 64$ MHz. Solid lines are bimodal fits of the satellite peaks, vertical dash-dotted lines mark their centers of gravity.

sists of two septets of relatively sharp quadrupole-split transitions, with positive ($B_0 < \nu_L/^{59}\gamma$) and negative offsets ($B_0 > \nu_L/^{59}\gamma$) of their respective central lines. The integrated amplitudes of the positive- and negative-offset multiplets are in a ratio very close to 2. Following the above arguments, the two multiplets originate from the majority spin-up and minority spin-down chains, respectively, in the presence of a sample misalignment of the order of a few degrees, yielding a longitudinal field component of order a few hundreds mT, strong enough to induce FI magnetic order in the sample.²⁴ The effect of sample rotation around an axis nominally coincident with the crystallographic c axis is summarized in Fig. 8, showing the dependence on the azimuthal angle ϕ of the central lines $B_{0\uparrow}$, $B_{0\downarrow}$, and of the first-order quadrupole splittings, calculated as $(B_{-1} - B_1)/2$.²³ Overlaid on the experimental points, the figure also shows for comparison simulated shifts (Fig. 8a) and splittings (Fig. 8b) predicted by Eqs. A2 and A3 for $\theta = 81^\circ$ (the angle between c and $B_{nuc} \approx B_{loc}$, resulting from a vector addition of $B_{ext} = 7.45$ T with a perpendicular $B_{int} \approx 1.2$ T), and rhombicity factors η of order 0.1. Clearly, the experimental splittings do not follow the predicted angular periodicity of π , rather showing a 2π period (Fig. 8a). Moreover, the quadrupolar shift is negligible even for large η values (Fig. 8b), since it is a second order term in ν_Q/ν_Z . Therefore, the entire azimuthal dependence of both quantities must be due to a slight misalignment between c and the rotation axis, as well as between the latter and the plane perpendicular to B_{ext} , indicating that η is vanishingly small.

The spectrum of Fig. 7 is fitted to two septets of Lorentzian lines, with constrained positions calculated as functions of external and internal fields, chemical shift,

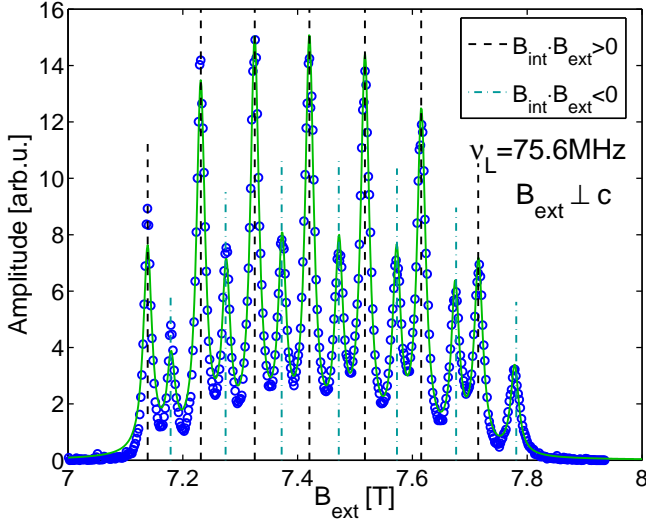


FIG. 7: (Color online) Field-swept spectrum at 10 K, recorded at a constant frequency of 75.6 MHz, in a nominally transverse geometry ($\mathbf{B}_{ext} \perp c$). The solid line is a global fit to two septets of Lorentzian lines with positions constrained by Eqn. A2. Vertical dashed and dash-dotted lines mark peak positions for the majority and minority spin chain signal, respectively.

quadrupole interaction, and a geometric angle α between the c axis and \mathbf{B}_{ext} . In the fit, the in-plane chemical shift tensor component K_a , α , and $\nu_{Q\uparrow}, \nu_{Q\downarrow}$ (which are in principle independent for the two chain types) were treated as free variational parameters, while $B_{int\uparrow}, B_{int\downarrow}$, and K_c were kept fixed to the values determined by NMR with $c \parallel B_{ext}$ (longitudinal geometry). A further constant parameter, $\rho \equiv d\psi/dB_{ext} = 3.4(2) \times 10^{-3} \text{ T}^{-1}$, accounting for a field-dependent tilting angle ψ of the electronic moments, was calculated from the ab -plane macroscopic susceptibility, determined by SQUID magnetometry as $\chi_{\perp} = 1.8(1) \times 10^{-2} \mu_B/\text{T}$. The fit yields a negative $K_a = -6.7(2) \times 10^{-3}$, and $\nu_{Q\uparrow} = \nu_{Q\downarrow} = 2.11(1) \text{ MHz}$, coincident with the quadrupole line splitting of the majority signal in the longitudinal geometry, and so is in disagreement with the value determined for the minority chains in large longitudinal fields.

B. Nuclear relaxations

Nuclear relaxations were systematically studied on the central quadrupole line ($m = 0$) in the longitudinal geometry ($\mathbf{B}_{ext} \parallel c$) at 10 K as a function of the external field. The longitudinal nuclear polarization recovers equilibrium in good agreement with Eqn. B2, indicating that spin-lattice relaxations are actually driven by magnetic fluctuations, as expected in this system.

Figure 9b displays spin-lattice and spin-spin relaxation rates of the positive-offset septet at 10 K over the 2-6 T field span, an interval comprising the FI-FM transition B_{c2} . Spin-spin rates T_2^{-1} are larger than spin-lattice rates

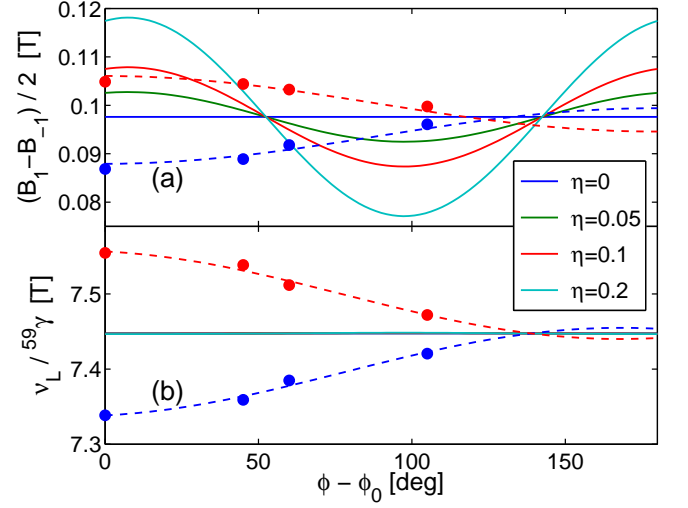


FIG. 8: (Color online) Symbols: experimental first order quadrupole splitting (a) and central peak position (b), in field units, as a function of the azimuthal angle ϕ in the transverse geometry. Dashed lines are guides to the eye. Solid lines: simulations with $\theta = 81^\circ$, corresponding to $\mathbf{B}_{ext} \perp c$ (see text and Eqn. A2), for increasing η values.

$T_1^{-1} \equiv 2W$ (Eqn. B2) by at least 3 orders of magnitude, and the two relaxations clearly follow quite different behaviors vs. B_{ext} . The former exhibits a peak at B_{c2} , with such a large maximum value that it nearly leads to the disappearance (wipeout) of the signal at this temperature. In contrast, T_1^{-1} exhibits a monotonic decrease with increasing fields, except for a shallow feature at B_{c2} . Moreover, the time dependence of the spin-spin relaxations exhibits a marked non-exponential decay over a wide field interval across the FI-FM transition. The signal decay is best fitted to a stretched exponential function, $A(\tau) = A_0 \exp[-(2\tau/T_2)^\beta]$, with stretching exponent β peaked to a value of 1.5 at B_{c2} , i.e. the intrinsic lineshape (related to the spin-spin relaxation function by Fourier transform) is nearly Gaussian close to the transition.

The difference in magnitude and field dependence of the T_1^{-1} and T_2^{-1} rates is not peculiar to the longitudinal orientation, as it can be qualitatively reproduced with the c axis rotated by $\alpha = 45^\circ$ in $B_{ext} = 4\text{--}7 \text{ T}$ (not shown), a field interval encompassing the FI-FM transition in that geometry. This indicates that the behavior of T_1^{-1} and T_2^{-1} vs. applied field is essentially invariant with respect to the orientation of the nuclear field $\mathbf{B}_{nuc} \approx \mathbf{B}_{loc}$ relative to the c axis (note that $B_{ext} \gg B_{int}$ in this case, so that the \mathbf{B}_{loc} direction is approximately that of \mathbf{B}_{ext}).

Perfectly consistent data are recorded from nuclei in the minority spin-down chains, for B_{ext} approaching B_{c2} from below. A qualitatively similar behavior of the two kinds of relaxations is also observed at 10 K close to the other metamagnetic transition, i.e. from the FI to the MPDA phase on decreasing the longitudinally applied B_{ext} down to $B_{c1} \approx 0.1 \text{ T}$ (Fig. 9a). Here again

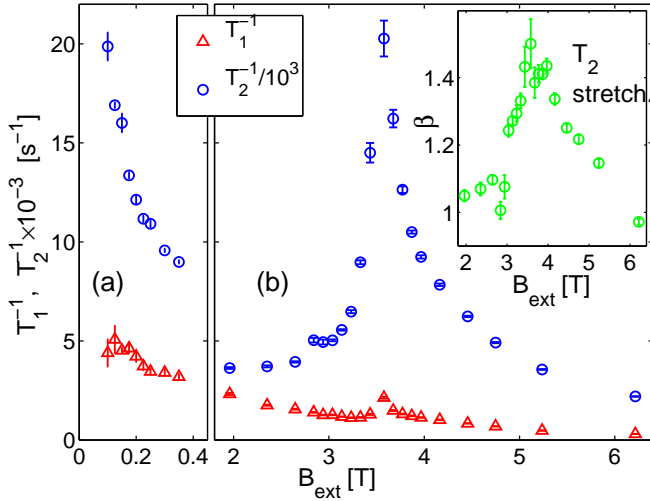


FIG. 9: (Color online) Spin-lattice (triangles) and spin-spin relaxations (bullets) measured on the central resonance of the positive-offset septet at 10 K as a function of $B_{ext} \parallel c$, (a) on approaching the FI-MPDA transition from above, and (b) across the FI-FM transition. Inset of panel b: stretching exponent β of the spin-spin relaxation function vs. B_{ext} . In the figure T_2^{-1} rates are scaled by a multiplication factor of 10^{-3} for clarity.

T_2^{-1} is orders of magnitude larger than T_1^{-1} and increases as B_{ext} approaches the critical field, while T_1^{-1} is non-divergent. As in the vicinity of B_{c2} , the homogeneous lineshape is quasi-Gaussian, as spin-spin relaxations are fitted to stretched exponential decay forms, with β in the range 1.2–1.4.

Spin-lattice relaxations were also measured as a function of temperature and applied field, both in the FI and FM phase. Results of a typical temperature scan, performed in a longitudinal field of 4.749 T (i.e. in the FM phase) are shown in Fig. 10. The figure also shows the temperature dependence of T_2^{-1} for comparison. The spin-lattice rate clearly follows a thermally activated behavior $T_1^{-1} = T_\infty^{-1} \exp(-\Delta/T)$, as also found by other authors.¹⁹ The Arrhenius law is obeyed over a temperature range of 8–13 K at this particular field, corresponding to a T_1 variation by more than two decades, with activation energy estimated as $\Delta = 96(2)$ K. Above this temperature interval the signal is lost due to an exceedingly short T_2 , while experimental T_1^{-1} points exhibit excess relaxation at $T < 8$ K, indicating that the relaxation mechanism responsible for the Arrhenius behavior becomes unimportant at low temperature, and it is shunted by other more effective relaxation channels. Spin-spin rates seemingly saturate at low temperature and also exhibit a steep temperature dependence at $T > 8$ K as well, although the evolution is clearly not Arrhenius-like.

Thermally activated $T_1^{-1}(T)$ were detected at *all fields*, irrespective of whether the system exhibits FI or FM order. The field dependence of the activation energy $\Delta(B_{ext})$, as well as its interpretation in terms of the el-

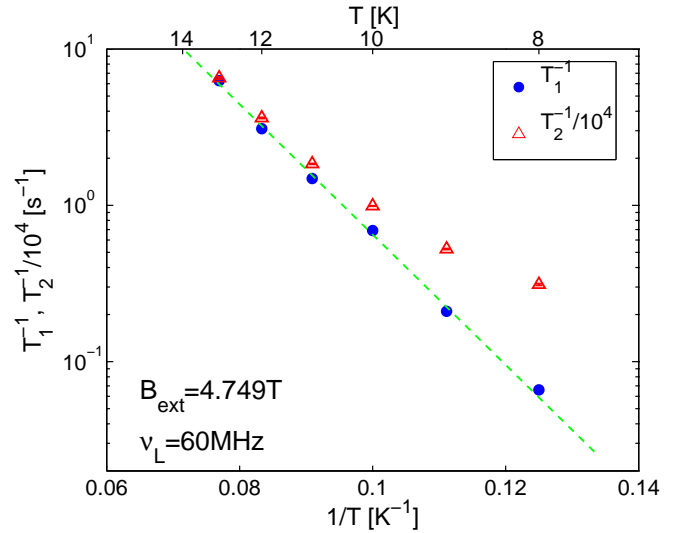


FIG. 10: (Color online) Spin-spin (triangles) and spin-lattice relaxation rates (bullets) measured in the FM phase on the central resonance ($\nu_0 = 60$ MHz, $B_{ext} = 4.749$ T parallel to c) as a function of temperature. The dashed line is a fit of T_1^{-1} to an Arrhenius law. In the figure T_2^{-1} rates are scaled by a multiplication factor of 10^{-4} for clarity.

ementary excitations of an Ising spin chain system, will be reported elsewhere.

IV. DIPOLAR FIELD CALCULATION

A calculation of the total dipolar field at the CoI site is required for a quantitative analysis of our experimental internal field values. We report such a calculation here for each of the three magnetic environments, majority FI-, minority FI-, and FM-ordered chains. The contribution of nearby moments (referred to as the proper dipolar field B_{dip}) is calculated by summing up the individual dipolar fields from CoII spins SS_j at positions \mathbf{r}_j inside a Lorentz sphere with a radius of several unit cell radius centered at a CoI site $\mathbf{r}_0 = 0$, $B_{dip} = \sum_j g\mu_B(3\mathbf{r}_j\mathbf{r}_j \cdot SS_j - r_j^2 SS_j)/r_j^5$, while spins outside the Lorentz sphere are treated as a macroscopic magnetic moment density, giving rise to a demagnetization field B_{dem} inside the sphere, as is customary. The latter is strictly constant throughout the sample volume only in the case of an ellipsoidal sample surface, whereby it is simply proportional to the saturation magnetization M_s and to the difference in demagnetizing factors of the inner Lorentz sphere $1/3$ and the outer sample surface N , $B_{dem} = 4\pi(1/3 - N)M_s$. For a rotational ellipsoid magnetized along its principal axis c , the demagnetizing factor N_c is calculated as²⁵

$$N_c = \frac{(1 - \epsilon^2)(\tanh^{-1} \epsilon - \epsilon)}{\epsilon^3} \quad (3)$$

$$\epsilon \equiv \sqrt{1 - (r_a/r_c)^2}$$

TABLE I: Calculated dipolar sum B_{dip} , demagnetization field B_{dem} , and total dipolar field $B_{tot} \equiv B_{dip} + B_{dem}$ as a function of magnetic chain ordering, compared with experimental B_{int} values.

Order	B_{dip} (T)	B_{dem} (T)	B_{tot} (T)	exp. (T)
FM	0.997	0.137	1.134	1.115(2)
FI \uparrow	1.122	0.046	1.167	1.178(2)
FI \downarrow	-1.246	0.046	-1.201	-1.221(4)

A non-ellipsoidal sample may be approximated by an effective ellipsoid accounting for the mean B_{dem} , while deviations from the ideal shape gives rise to a distribution in demagnetization fields, contributing only to the linewidth. We assume effective ellipsoid radii $r_a = r_b$, r_c equal to half of the sides of our square-base parallelepipedal specimen as a best ellipsoidal approximation. The choice of r_a and r_c does not critically affect the determination of B_{dem} , since N_c depends weakly on ϵ in the case of an elongated sample (e.g. $\partial N_c / \partial \epsilon \approx 0.3$ for our crystal). For instance, a 10% error on ϵ would result in an error ΔB_{dem} of order 5 and 2 mT in the FM and FI phases, respectively.

The results of our calculations are summarized in table I and compared with experimental results. Both the dipolar sums and the demagnetization field were calculated by assuming the CoII moments saturated to $\pm g \langle S_z \rangle \mu_B$ along c in all the three types of magnetic chains, with a \pm sign as appropriate for the chain order, and identical absolute moment values estimated as $g \langle S_z \rangle = 5.25(3)$ (in units of μ_B) from an extrapolation of $M(H)$ data in high field. Lattice parameters were taken as $a = 9.061 \text{ \AA}$, $c = 10.367 \text{ \AA}$ as reported in the literature at 40 K.¹ Numerical convergence of B_{dip} could be attained with a Lorentz sphere radius of the order 30 of unit cells. Calculated and experimental values differ by less than 2% in all cases. Agreement should be considered satisfactory in view of the uncertainties in the magnetic moment (of order 1%) and the demagnetization factor. This confirms that the internal field is dipolar in origin, while transferred hyperfine contributions, if they occur, are negligible.

V. DISCUSSION AND CONCLUSIONS

We organize the discussion of our experimental results into separate sections for sake of clarity, each one focusing on one main conclusion of the paper.

A. Interactions of ^{59}Co : evidence against a direct Co I-Co II superexchange path

Our NMR study on a single-crystal provides a determination of the chemical shift and the EFG tensors at the CoI site. The chemical shift is less precise due to the uncertainty in the zero-shift ^{59}Co reference²⁶ and to

the presence of a large internal field which complicates the unraveling of \hat{K} components (see Appendix A). The absolute magnitude of K , of order 1%, though sizable in absolute terms, is however only slightly larger than the typical values reported for diamagnetic complexes of cobalt.²⁷ The relatively small value of K agrees with the known large crystal field splitting at the octahedral I site, of order 0.65 eV,³ since a near-lying crystal field excited multiplet usually gives rise to a large chemical shift via the van-Vleck mechanism, as often encountered in non-magnetic transition metal ions.

The EFG exhibits cylindrical symmetry around c , in accordance with the fact that c axis is a C_3 symmetry element of the point group of CoI. Consistent values of the quadrupolar frequency ν_Q (proportional to the EFG) are estimated in different chain types and experimental geometries, with the notable exception of the minority chains in external longitudinal fields approaching the FI-FM transition value B_{c1} , where an EFG deviation of order -7% is found, well beyond the experimental uncertainty. We argue that a magnetoelastic coupling of the Co^{3+} ions in counter-oriented minority chains might be the source of the observed EFG reduction, as already proposed for other cobalt-based compounds studied by Mössbauer spectroscopy.²⁸

The internal field B_{int} at the non-magnetic CoI site can be accounted for by purely dipolar interactions with the surrounding CoII spins, within an absolute accuracy of 2 mT in all of the three chain types. This result, along with the experimental value of \hat{K} , sets a very stringent upper limit to a transferred hyperfine field at the nucleus.

The contact hyperfine field may originate from both a tiny on-site magnetic moment on CoI, as that invoked in a neutron scattering refinement,⁷ and from the coupling to nearest neighbors CoII spins. These two contributions might partially cancel out, since either sign is possible.²² Additional inter-chain contributions are negligible in view of the large chain spacing. Nevertheless, we can safely rule out an on-site term, since a residual on-site moment would require an admixture of the t_{2g} with the excited e_g orbitals, in contrast with the large crystal field excitation energy implied by the observed moderate chemical shift value. For instance, a huge chemical shift $K \approx 5$ was reported for the resonance of ^{141}Pr in low-spin Pr^{3+} , in combination with a small fractional moment $\approx 0.01 \mu_B$ on the Pr ion.²⁹ Therefore, only the transferred contribution is to be considered.

An intra-chain transferred hyperfine term B_{hf} would offset the total dipolar field B_{tot} (Tab. I) by $\pm |B_{hf}|$ for the FI \uparrow and FM chains, and by $\mp |B_{hf}|$ for the FI \downarrow chains, depending on the relative sign of B_{tot} and B_{hf} . However, a finite B_{hf} biasing term does not improve the agreement between the calculated $B_{tot} \pm B_{hf}$ and the experimentally determined internal fields. We conclude therefore that the slight discrepancy between the experimental and the calculated internal fields must be due to other sources of error, and that the contact field, if present, is much smaller than 2 mT.

A negligible hyperfine field at the CoI site is an unexpected result. Transferred hyperfine fields at nuclei of non-magnetic ions in magnetic compounds of transition metals are typically of the order of several hundreds mT or more, unless perfect cancellation occurs at a symmetric site of an AF structure, which is not the case in $\text{Ca}_3\text{Co}_2\text{O}_6$. For instance, the transferred hyperfine field at ^{139}La in the FM manganite $\text{La}_{1-x}\text{Ca}_x\text{MnO}_3$ equals 3 T, i.e. approximately 10% of the on-site hyperfine field at the Mn sites, where the magnetism resides.³⁰ Here, a virtually vanishing contact field at CoI indicates that there is no significant hybridization between the Co^{3+} (I) and the Co^{3+} (II) wave functions either directly or through an oxygen bridge.

The mechanisms underlying exchange and hyperfine transfer are similar, although not exactly identical.^{31,32} Therefore, the lack of a detectable transferred hyperfine field strongly suggests that Co^{3+} (I) ions do not participate in the exchange interaction J_1 between two neighboring on-chain Co^{3+} (II) spins. We stress that this finding constitutes experimental evidence against the currently accepted theoretical model by Frésard *et al.*, who instead proposed an exchange path across CoI assuming a large overlap of Co^{3+} (II) with Co^{3+} (I) wave functions, yielding a direct integral $t = 1.5\text{ eV}$.³³

B. Nature of the metamagnetic transitions: perfect Ising behavior.

At 10 K two types of field-dependent magnetic structures are detected, namely perfect FI and FM ones, in accordance with the two plateaus in magnetization data at the same temperature. The two structures are clearly identified by distinct local fields at the CoI sites in good quantitative agreement with the dipolar fields calculated for the corresponding spin arrangements. The transition from a FI to a FM phase shows up as a sharp step in B_{int} at a threshold field $B_{c2} \approx 3.5\text{ T}$, revealed by an abrupt crossover of the resonance frequency vs. field between two distinct $\nu_0(B_{ext})$ functions (Fig. 3).

Quantitative comparison between NMR and magnetization data in longitudinal fields at 10 K (Fig. 11) provides an insight into the magnetization process. Close inspection of the magnetization curves as a function of the applied field $H \equiv B_{ext}/\mu_0$ shows that the steps appear smoother in the $M(H)$ curves than in the NMR frequency data $\nu_0(B_{ext})$ (figure inset). Moreover, the plateaus in $M(H)$ are only approximately flat, with a moderate field dependence that is larger in the FI state (for instance, $\mu_0^{-1}\partial M/\partial H \approx 0.05\mu_B/\text{T}$ for $1\text{ T} < \mu_0 H < 3\text{ T}$).

In principle, incomplete saturation of $M(H)$ over the plateaus might be due to either unsaturated c axis components of individual moments in a homogeneously magnetized sample (e.g. due to spin canting), or inhomogeneous magnetization, although the former could not easily be reconciled with the known strong single ion anisotropy of the system. NMR demonstrates experimentally that the cobalt spins are collinear and saturated

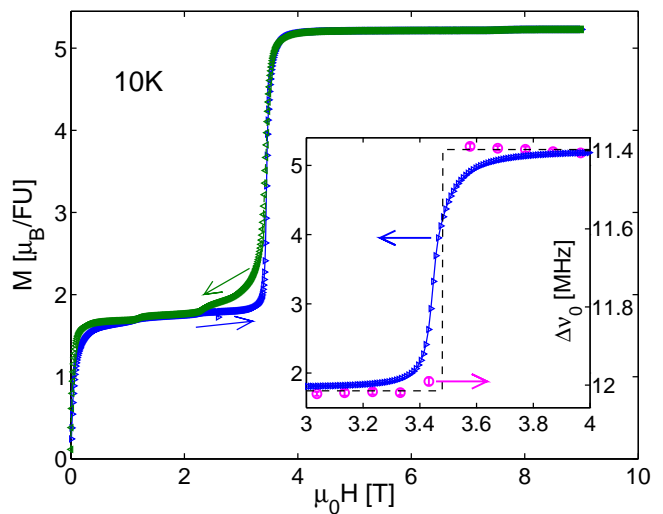


FIG. 11: (Color online) Magnetization curves at 10 K as a function of the external field H applied along c . Inset: detail of $M(H)$ across the FI-FM transition, overlaid for comparison to the frequency offsets $\Delta\nu_0 \equiv \nu_0 - aB_{ext}$ of the central NMR line of either FI \uparrow or FM chains, where a is the best-fit parameter to Eqn. 1 (whence $\Delta\nu_0 \approx b \propto B_{int}$ within error).

even in the vicinity of the FI-FM transition. Proof is provided by the field proportionality coefficient a of Eqn. 1, whose experimental values for the three chain types were found to coincide within an error $\delta a \approx 10\text{ kHz/T}$. The observed value of $\partial M/\partial H$ contributes a 15 kHz/T slope (i.e. of order δa) to $\nu_0(B_{ext})$ via the demagnetization field, regardless of the mechanism responsible for it, and independent of the magnetic order in a chain. A hypothetical field dependent canting, however, would affect the dipolar field at CoI, which is larger than the demagnetization field by an order of magnitude (Tab. I). Unless we assume equal canting in the FM, FI spin-up, and the FI spin-down chains, which is clearly unphysical, the latter would produce differences in the a coefficients of the three lines well beyond experimental errors, and contrary to experimental evidence.

As seen from NMR, the system apparently exhibits perfect Ising behavior. Therefore, the rounded steps in the $M(H)$ data at the field-induced metamagnetic transitions, with unsaturated magnetization over broad H intervals near them, must be due to a fraction of misoriented domains or spin chains.

C. Two distinct magnetic excitations probed by T_1^{-1} and T_2^{-1}

Further insight on the spin reversal process close to the MPDA-FI and FI-FM transitions is provided by the large and divergent spin-spin relaxations, accompanied by much smaller and non-divergent spin-lattice relaxations. We recall that the spin-lattice relaxation rate T_1^{-1} probes transverse random magnetic fields fluctuating at the Larmor frequency ω_L , while the spin-spin rate

T_2^{-1} is the sum of a term proportional to T_1^{-1} (the population term) and a secular term arising from longitudinal random fields fluctuating at virtually zero frequency.^{34,35} In the presence of isotropic and fast fluctuations in the so-called narrowing limit (such that ω_L is much smaller than the roll-off frequency of the fluctuation spectrum) the two rates tend to coincide.³⁶ Here, the similar behavior of relaxations measured in longitudinal and oblique external fields rules out the possibility that anisotropic fluctuations, namely, entirely along the c axis and hence ineffective for spin-lattice relaxations, are the source of the huge difference in T_1 and T_2 time scales. Excess spin-spin relaxation and T_2^{-1} peaks must instead depend on fluctuations in a regime opposite to the narrowing limit, namely with characteristic frequencies much lower than ω_L and hence contributing only to the secular term in T_2^{-1} . Such a regime, which has already been reported in the literature for other oxides,³⁷ is referred to hereafter as the nearly-static limit.

To this end, the Kubo-Tomita theory of line shape appropriate for continuous-wave magnetic resonance³⁸ is modified in the context of pulsed NMR by an experimental low-frequency cutoff, namely the reciprocal time window $\omega_c = (2\tau)^{-1}$ of a spin-echo experiment (here, τ is the time separation of the two excitation pulses). Random fields fluctuating at frequencies $\omega \ll \omega_c \approx 2 \times 10^4 \text{ s}^{-1}$ may be viewed as static over the excitation-detection transient and contribute only to the inhomogeneous line broadening, which is refocused by the spin echo sequence. Conversely, fluctuations at $\omega_c < \omega \ll \omega_L$ effectively relax the spin-echo signal.

Within the nearly-static limit, the decrease of T_2^{-1} with decreasing temperature (Fig. 10) then indicates the collapse of the fluctuation spectrum below the cutoff ω_c at lower temperatures, down to a complete freezing of the spin dynamics observed at $T < 5 \text{ K}$. It is worth noting that evidence for comparable time scales in the spin dynamics was also reported from χ' and χ'' ac magnetic susceptibilities in the zero-field phase, both showing a strong frequency dependence over the acoustic and sub-acoustic range.³⁹ The nearly Gaussian T_2 relaxation form is another signature of nuclear spin depolarization from quasi static random fields.³⁴ In our case, random fields are clearly electronic in origin, since the calculated second moment of the nuclear dipolar fields yields a T_2^{-1} rate smaller than the observed ones by at least one order of magnitude.

The peculiar behavior of T_2^{-1} rates therefore reflects the exceedingly slow spin dynamics, as in the case of massive excitation modes involving the collective motion of several spins. In view of the strong Ising character of the system, such excitations probably consist in the coherent reversal of large portions of the spin chains or domains. The slowly fluctuating random fields responsible for spin-spin relaxation are then straightforwardly identified with the stray dipolar fields originating from such transient defects in the magnetic structure. Also the peaks in T_2^{-1} and the stretched exponent β at the meta-

magnetic transitions finds a natural explanation within this framework.

A peak in T_2^{-1} vs. B_{ext} may arise in principle from either a field-dependent correlation time of fluctuations, or a peak in the random field amplitude. In the nearly-static fluctuation regime, however, field dependence of the correlation time would imply *faster* spin fluctuations at the peak. The latter is apparently inconsistent with the peaks in β vs. B_{ext} reaching nearly-Gaussian values of 1.5 at B_{c1} and B_{c2} , a signature of a nearly frozen spin dynamics, following the above argument. The T_2^{-1} peak must therefore originate from a corresponding increase of the quasi-static magnetic disorder, namely a larger number of misoriented domains or chain fragments, close to the transitions. We note that the peaks of β vs. B_{ext} coherently reflect changes in the spatial distribution of random fields on approaching the metamagnetic transitions. According to a well-known mechanism,^{34,40} the transition from a quasi-Gaussian to a quasi-Lorentzian line shape may be driven by an increasing dilution of (nearly) static magnetic impurities or defects, and vice versa. Thus, the larger disorder probed by T_2^{-1} peaks consistently coincides with a larger concentration of magnetic defects indicated by $\beta > 1$, which agrees with the shortening of the magnetic coherence length observed on approaching the field-induced transitions.⁴¹

In contrast, spin-lattice relaxations are governed by independent excitations, whose effect on T_2 is unimportant as it is masked by the relaxation channel sketched above. The thermally activated behavior of T_1^{-1} reveals a *gap* Δ of order 100 K in their spectrum. A thorough investigation of Δ as a function of B_{ext} for the different chain types, and a fitting of the experimental energy gaps to a theoretical model, are the subject of a separate paper. Here we anticipate that, according to the model, the activated spin-lattice relaxations are essentially driven by the spin-flip of a single Co^{3+} moment.

D. Spin freezing: relevance for the magnetization steps

We conclude this discussion with a comment on the low-temperature multi-step behavior in $M(H)$. The magnetic structures underlying each step could not be accessed in our NMR study, due to the non-spherical shape of our sample, inducing demagnetization-dependent line broadening and offsets which prevent finer resolution of dipolar fields, as well as to exceedingly slow spin-lattice relaxations below 5 K. Nevertheless, T_2 data at 7-15 K reveal a scenario of glassy spin dynamics involving freezing of sizable magnetic aggregates and large quasi-static inhomogeneities close to the field-induced transitions. The collective arrangement of such frozen entities at lower temperature is unknown. We may argue however that it gives rise to complex field-dependent micromagnetic configurations or superstructures, resulting in a multiplicity of local minima separated by potential barriers in the free energy, becoming metastable below 2 K. If this

picture holds true, however, the physical mechanism behind magnetization steps should be understood in terms of thermally assisted hopping between essentially mesoscopic metastable configurations, probably incommensurate with the crystal lattice, rather than quantum tunneling as in molecular magnets.

ACKNOWLEDGMENT

The authors thank S. Carretta and P. Santini for helpful and stimulating discussion.

Appendix A: The ^{59}Co resonance

The resonance frequencies of ^{59}Co at the non-magnetic site I, for an arbitrary experimental geometry, depend on the external field and sample alignment in a rather complicated way, which deserves some comment.

The field at the nucleus \mathbf{B}_{nuc} (proportional to the resonance frequency $\nu_Z = \gamma B_{nuc}$) differs from the local field \mathbf{B}_{loc} at the ion site by the chemical shift, $\mathbf{B}_{nuc} = (1 + \hat{K})\mathbf{B}_{loc}$, where the chemical shift tensor \hat{K} is usually large and anisotropic in cobalt.²⁷ In a magnetic material, the local field is the vector composition of the external and the internal field, $\mathbf{B}_{loc} = \mathbf{B}_{ext} + \mathbf{B}_{int}$, where the internal field \mathbf{B}_{int} originates from the electronic moments. The overall dependence of ν_Z is summarized by Eqn. 2.

In the present case, the sources of \mathbf{B}_{int} are *i)* the dipolar coupling with neighboring Co II spins; *ii)* the net demagnetization field, namely, the difference between the demagnetization effects of the outer sample surface and a Lorentz sphere, which does not vanish due to the non-spherical shape of the sample; and *iii)* possibly, a transferred hyperfine contribution, due to the polarization of wave functions. Even in a hard easy-axis magnet like the present one, the direction of magnetic moments with respect to the crystal axes, hence of \mathbf{B}_{int} , depends on $\mathbf{H} \approx \mu_0^{-1} \mathbf{B}_{ext}$ via the finite transverse magnetic susceptibility χ_{ab} of the system, leading to a field-induced tilting of the Co^{3+} spins by a small but non-negligible angle $\psi \propto \chi_{ab} H_{\perp}$, and by $\approx -\psi/2$ for \mathbf{B}_{int} , if the dipolar contribution dominates.

In a crystal, ^{59}Co ($I = 7/2$) is also coupled by its quadrupole moment to the local electric field gradient (EFG) via a quadrupolar spin Hamiltonian of the form

$$\mathcal{H}_Q = \frac{h\nu_Q}{6} \left[3I_z^2 - I(I+1) + \frac{\eta}{2} (I_+^2 + I_-^2) \right] \quad (\text{A1})$$

where $I_{\pm} = I_x \pm iI_y$, and I_x, I_y, I_z are the nuclear spin components in the crystal reference frame. Here the quadrupolar frequency ν_Q is defined as a function of the nuclear quadrupole moment Q and the main component V_{zz} of the EFG tensor as $\nu_Q = 3eV_{zz}Q/[2hI(2I-1)]$, and $\eta = ||V_{yy}| - |V_{xx}||/V_{zz}$ is the EFG rhombicity factor.³⁴

In the presence of a large magnetic field (either external or internal) at the nucleus, such that $\nu_Z \gg \nu_Q$, the quadrupolar interaction of Eqn. A1 behaves as a perturbation, and splits the nuclear Zeeman transitions into a multiplet of $2I$ satellite lines. In a second-order expansion vs. ν_Q/ν_Z , the frequency ν_n of the $|n-1/2\rangle \leftrightarrow |n+1/2\rangle$ Zeeman transition ($n = -2I + 1/2, -2I + 3/2, \dots, 2I - 1/2$) depends on \mathbf{B}_{nuc} as

$$\begin{aligned} \nu_n = \nu_Z - \frac{4\nu_Q^2}{\nu_Z} \left[(I+1/2)^2 - 1 \right] [2\mathcal{B}(\theta, \phi) - \mathcal{C}(\theta, \phi)] - \\ \nu_Q \mathcal{A}(\theta, \phi) n + \frac{12\nu_Q^2}{\nu_Z} [4\mathcal{B}(\theta, \phi) - \mathcal{C}(\theta, \phi)] n^2 \end{aligned} \quad (\text{A2})$$

where θ, ϕ are the polar coordinates of \mathbf{B}_{nuc} in the crystal frame, and the coefficients $\mathcal{A}, \mathcal{B}, \mathcal{C}$ are defined as

$$\begin{aligned} \mathcal{A}(\theta, \phi) &= \frac{1}{2} (3 \cos^2 \theta - 1 + \eta \sin^2 \theta \cos 2\phi) \\ \mathcal{B}(\theta, \phi) &= \frac{1}{144} \sin^2 \theta [\cos^2 \theta (9 - 6\eta \cos 2\phi + \eta^2 \cos^2 2\phi) \\ &\quad + \eta^2 \sin^2 2\phi] \\ \mathcal{C}(\theta, \phi) &= \frac{1}{576} \{ 9 \sin^4 \theta + 6\eta \sin^2 \theta (1 + \cos^2 \theta) \cos 2\phi + \\ &\quad \eta^2 [\cos^2 2\phi + 2 \cos^2 \theta (1 + \sin^2 2\phi) + \cos^2 \theta \cos^2 2\phi] \} \end{aligned} \quad (\text{A3})$$

We note that all second order terms vanish for a cylindrical EFG ($\eta = 0$) and EFG principal axis collinear to \mathbf{B}_{nuc} ($\theta = 0$).

Appendix B: The spin-lattice relaxation function

The approach to thermodynamic equilibrium of an ensemble of nuclear spins I is governed by a closed set of rate equations for the m -th level population N_m ($m = I, \dots, -I$). In the presence of a magnetic relaxation channel, it has the form⁴²

$$\begin{aligned} \dot{N}_m = & W[(I+m+1)(I-m)(N_{m+1} - N_{m+1}^{(0)}) \\ & + (I-m+1)(I+m)(N_{m-1} - N_{m-1}^{(0)}) \\ & - 2(I^2 - m^2 + I)(N_m - N_m^{(0)})] \end{aligned} \quad (\text{B1})$$

where $N_m^{(0)}$ is the population at equilibrium, and W is the transition probability $|m\rangle \leftrightarrow |m-1\rangle$ between two adjacent Zeeman levels. In the case of quadrupole-split NMR lines with the selective excitation of a single nuclear transition of order n ($n = I - 1/2, \dots, -I + 1/2$), the signal intensity is proportional to the population difference $A_n \equiv N_{n+1/2} - N_{n-1/2}$ of the two levels involved, rather than the expectation value of the total spin $\langle I_z \rangle$. Solution of Eqn. B1 yields a recovery of A_n according to the superposition of $2I$ exponential components for generic n (reduced to $I + 1/2$ for $n = 0$) with relative

weights depending on the saturation method as well as on n .

In our experiments, the spin ensemble was prepared with a fast saturation, i.e. with a pulse train much shorter than the spin-lattice relaxation time $T_1 \equiv (2W)^{-1}$, so that populations N_m of nuclear levels $m \neq n \pm 1/2$ not involved in the transition were practically unaffected.^{42,43} For the central line $n = 0$ of a $I=7/2$ nuclear species as ^{59}Co , the recovery law following such an initial condition

is then calculated as follows.

$$A_0(t) = A_0^{(0)} \left(1 - \frac{1}{84} e^{-2Wt} - \frac{3}{34} e^{-12Wt} - \frac{150}{728} e^{-30Wt} - \frac{1225}{1716} e^{-56Wt} \right) \quad (\text{B2})$$

* Electronic address: allodi@fis.unipr.it

- ¹ H. Fjellvåg, E. Gulbrandsen, S. Aasland, A. Olsen, and B. C. Hauback, *J. Solid State Chem.* **124**, 190 (1996).
- ² A. Maignan, C. Michel, A. C. Masset, C. Martin, and B. Raveau, *Eur. Phys. J. B* **15**, 657 (2000).
- ³ T. Burnus, Z. Hu, M. W. Haverkort, J. C. Cezar, D. Flahaut, V. Hardy, A. Maignan, N. B. Brookes, A. Tanaka, H. H. Hsieh H.-J. Lin, C. T. Chen, and L. H. Tjeng, *Phys. Rev. B* **74**, 245111 (2006).
- ⁴ E. V. Sampathkumaran, N. Fujiwara, S. Rayaprol, P. K. Madhu, and Y. Uwatoko, *Phys. Rev. B* **70**, 014437 (2004).
- ⁵ R. Vidya, P. Ravindran, H. Fjellvåg, A. Kjekshus, and O. Eriksson, *Phys. Rev. Lett.* **91**, 186404 (2003).
- ⁶ Hua Wu, M. W. Haverkort, Z. Hu, D. I. Khomskii, and L. H. Tjeng, *Phys. Rev. Lett.* **95**, 186401 (2005).
- ⁷ S. Aasland, H. Fjellvåg, and B. Hauback, *Solid State Commun.* **101**, 187 (1997).
- ⁸ M. Mekata, *J. Phys. Soc. Jpn.* **42**, 76 (1977).
- ⁹ K. Wada and T. Ishikawa, *J. Phys. Soc. Jpn.* **52**, 1774 (1983).
- ¹⁰ H. Kageyama, K. Yoshimura, K. Kosuge, H. Mitamura, and T. Goto, *J. Phys. Soc. Jpn.* **66**, 1607 (1997); H. Kageyama, K. Yoshimura, K. Kosuge, X. Xu, , and S. Kawano, *ibid.* **67**, 357 (1998).
- ¹¹ O. A. Petrenko, J. Wooldridge, M. R. Lees, P. Manuel, and V. Hardy, *Eur. Phys. J. B* **47**, 79 (2005).
- ¹² S. Agrestini, C. Mazzoli, A. Bombardi, and M. R. Lees, *Phys. Rev. B* **77**, 140403(R) (2008).
- ¹³ S. Agrestini, L. C. Chapon, A. Daoud-Aladine, J. Schefer, A. Gukasov, C. Mazzoli, M. R. Lees, and O. A. Petrenko, *Phys. Rev. Lett.* **101**, 097207 (2008).
- ¹⁴ A. Maignan, V. Hardy, S. Hebert, M. Drillon, M. R. Lees, O. Petrenko, D. Mc K. Paul, and D. Khomskii, *J. Mater. Chem.* **14**, 1231 (2004).
- ¹⁵ V. Hardy, M. R. Lees, O. A. Petrenko, D. McK. Paul, D. Flahaut, S. Hébert, and A. Maignan, *Phys. Rev. B* **70**, 064424 (2004).
- ¹⁶ Y. B. Kudasov, *Phys. Rev. Lett.* **96**, 027212 (2006).
- ¹⁷ V. Hardy, S. Lambert, M. R. Lees, and D. McK. Paul, *Phys. Rev. B* **68**, 014424 (2003).
- ¹⁸ G. Allodi, A. Banderini, R. De Renzi, and C. Vignali, *Rev. Sci. Instrum.* **76**, 083911 (2005).
- ¹⁹ Y. Shimizu, M. Horibe, H. Nanba, T. Takami, and M. Itoh, *Phys. Rev. B* **82**, 094430 (2010).
- ²⁰ C. S. Lue, Y. T. Lin, and C. N. Kuo, *Phys. Rev. B* **75**, 075113 (2007).
- ²¹ M. Pieper, H. Niki, U. Seto, E. Gratz, K. Hense, N. Stuesser, V. Paul-Boncour, A. S. Markosyan, and A. Hoser, *J. Magn. Mater.* **272-276**, E389 (2004).
- ²² H. Yoshie, and Y. Nakamura, *J. Phys. Soc. Jpn.* **57**, 3157

- (1988).
- ²³ Hereafter we denote as B_n the position of the n -th quadrupole satellite in a field sweep spectrum at a fixed frequency ν_L , implicitly defined by the equation $\nu_n(B_n) - \nu_L = 0$, where $\nu_n(B_{ext})$ is the resonance frequency of the n -th satellite in an external field B_{ext} .
- ²⁴ We remark that powder average of line patterns like the present ones would actually lead to NMR spectra with “more than one [signal] with different centers of gravity”, as pointed out by Ref. 4. However, their bimodal spectra simply reflect the presence of a FI volume fraction in the sample, whereby majority and minority chains give rise to positive and negative internal fields, respectively.
- ²⁵ L. D. Landau and E. M. Lifshitz, *Electrodynamics of Continuous Media*, 2nd edition, Pergamon, New York (1984).
- ²⁶ The ^{59}Co gyromagnetic ratio is determined as $^{59}\gamma/2\pi = 10.10 \text{ MHz/T}$ from a $\text{K}_3\text{Co}(\text{CN})_6$ aqueous solution reference, see e.g. Ref. 20. In the literature there is however large dispersion in the reported values for $^{59}\gamma$, due to the large chemical shifts of ^{59}Co and the uncertainty on a zero-shift reference.²⁷
- ²⁷ J. C. C. Chan, and S. C. F. Au-Yeung, *Annu. Rep. NMR Spectro.* **41**, 1 (2000).
- ²⁸ D. C. Price, B. D. Howes, and M. C. K. Wiltshire, *J. Phys. C: Solid State Phys.* **17**, 3645 (1984).
- ²⁹ K. Nehrke, and M. W. Pieper, *Phys. Rev. Lett.* **76**, 1936 (1996).
- ³⁰ G. Allodi, R. De Renzi, F. Licci, and M. W. Pieper, *Phys. Rev. Lett.* **81**, 4736 (1998).
- ³¹ P. W. Anderson, *Exchange in Insulators: Superexchange, Direct Exchange, and Double Exchange*, in *Magnetism I*, eds. G. T. Rado, H. Suhl, Academic Press, New York (1963).
- ³² A. J. Freeman and R. E. Watson, *Hyperfine Interactions in Magnetic Materials*, in *Magnetism IIA*, eds. G. T. Rado, H. Suhl, Academic Press, New York (1965).
- ³³ R. Frésard, C. Laschinger, T. Kopp, and V. Eyert, *Phys. Rev. B* **69**, 140405(R) (2004).
- ³⁴ A. Abragam, *The Principles of Nuclear Magnetism*, Clarendon Press, Oxford (1961).
- ³⁵ C. P. Slichter, *Principles of Magnetic Resonance*, Springer, New York (1990).
- ³⁶ In the present case of EFG-perturbed NMR with resolved quadrupole satellites, rate equations predict an asymptotic constant ratio T_2^{-1}/T_1^{-1} larger than unit, equal to 16 for the central line of ^{59}Co ($I = 7/2$). See e.g. R. R. Ernst, G. Bodenhausen, and A. Wokaun, *Principles of Nuclear Magnetic Resonance in One and Two Dimensions*, Oxford Univ. Press, Oxford (1987) p. 55.
- ³⁷ G. Allodi, M. Cestelli Guidi, R. De Renzi, A. Caneiro, and

- L. Pinsard, Phys. Rev. Lett. **87**, 127206 (2001).
- ³⁸ R. Kubo, and K. Tomita, J. Phys. Soc. Japan **9**, 888 (1954).
- ³⁹ V. Hardy, D. Flahaut, M.R. Lees, and O.A. Petrenko, Phys. Rev. B **70**, 214439 (2004).
- ⁴⁰ R.E. Walstedt, and L.P. Walker, Phys. Rev. B **9**, 4857 (1974).
- ⁴¹ C. Mazzoli, A. Bombardi, S. Agrestini, and M.R. Lees, Physica B **404**, 3042 (2009).
- ⁴² A. Narath, Phys. Rev. **162**, 320 (1967).
- ⁴³ T. Rega, J. Phys.: Condens. Matter **3**, 1871 (1991).